

Denys DUTYKH

CNRS, Université Savoie Mont Blanc, France

Jean-Guy CAPUTO

INSA de Rouen, France

WAVE DYNAMICS ON NETWORKS:
METHOD AND APPLICATION TO THE
SINE–GORDON EQUATION

arXiv:1506.02405v3 [math-ph] 6 Feb 2018

LAST MODIFIED: February 7, 2018

WAVE DYNAMICS ON NETWORKS: METHOD AND APPLICATION TO THE SINE–GORDON EQUATION

DENYS DUTYKH* AND JEAN-GUY CAPUTO

ABSTRACT. We consider a scalar HAMILTONIAN nonlinear wave equation formulated on networks; this is a non standard problem because these domains are not locally homeomorphic to any subset of the EUCLIDEAN space. More precisely, we assume each edge to be a 1D uniform line with end points identified with graph vertices. The interface conditions at these vertices are introduced and justified using conservation laws and an homothetic argument. We present a detailed methodology based on a symplectic finite difference scheme together with a special treatment at the junctions to solve the problem and apply it to the sine–GORDON equation. Numerical results on a simple graph containing four loops show the performance of the scheme for kinks and breathers initial conditions.

Key words and phrases: Partial differential equations on networks; HAMILTONIAN partial differential equations; graph theory; sine–GORDON equation

MSC: [2010] 35R02 (primary), 34B45 (secondary)

PACS: [2010] 05.45.Yv (primary), 74.81.Fa (secondary)

Key words and phrases. Partial differential equations on networks; HAMILTONIAN partial differential equations; graph theory; sine–GORDON equation.

* Corresponding author.

CONTENTS

1	Introduction	5
2	Continuous sine–Gordon equation	6
2.1	Variational structure	6
2.2	Exact solutions	7
2.3	Coupling conditions at the junctions	8
	Back-to-Manifold: a homothetic approach	9
	Conservation laws approach	11
3	Numerical implementation : the discrete sine-Gordon equation	13
3.1	Formulation on graphs	15
3.2	Conditions on junctions: the discrete case	17
3.3	The numerical algorithm	17
4	Numerical results	18
4.1	Propagation of kinks	18
4.2	Propagation of a breather	21
	Weak energy breather evolution	24
5	Conclusions and perspectives	24
	Acknowledgments	27
A	Conservation laws approach	27
	References	28

1. Introduction

Currently there is a growing demand for modelling and understanding various flow problems on networks. A generic network is a (usually finite) set of points or simply *vertices* immersed in an EUCLIDEAN space \mathbb{E}^2 or \mathbb{E}^3 (depending on the application in hands). Some of the points are connected by 1D segments (or more generally curves, which are homeomorphic to segments), called the *edges*. Mathematically networks are formalized using graph theory [16]. However, there is an important subtle difference with graph theory. Namely, in some applications the geometry of edges (*e.g.* their length, shape, thickness) may matter, while in graph theory the only relevant information is the fact that two points are connected by an edge. Such sensitive applications include, for example blood flow modelling [38]. Thus, a network combines in a single data structure the corresponding geometrical and topological information on vertices and edges. The flow is modeled with Partial Differential Equations (PDEs) because of the spatial dimension of the edges, as opposed to Ordinary Differential Equations (ODEs) in the standard case. For a general recent review of this topic, see [7]. This field continues to attract researchers from modelling, analysis, numerics, optimization and control theory [41].

One of the main difficulties of formulating evolution problems described by PDEs on networks (*i.e.* graphs) consists in the fact that these objects are not manifolds. Recall that an n -dimensional manifold is such that each point has a neighborhood that is homeomorphic to \mathbb{R}^n [2]. Nowadays, the formulation of HAMILTONIAN mechanics on manifolds does not pose any serious technical difficulties [4]. However, the modeling of various processes on networks, such as electric circuits, blood arteries, water-pipe supply needs the generalization of classical mechanics to non-manifolds like graphs and trees. Consider, for example, a Y - or T -junction. This domain is a *semi-algebraic set*, but not a *manifold*. The difficulty comes from the branching point whose neighbourhood is not *homeomorphic* to any EUCLIDEAN space \mathbb{E}^k . Therefore any composition of Y -junctions into, for example, a complex tree will not be a manifold either.

To our knowledge, HAMILTONIAN problems on non-manifolds have not been systematically studied. A notorious exception is the work [5], where wave scattering in the KLEIN-GORDON(-FOK) equation was investigated on a domain consisting of three semi-infinite straight lines having one common point. We can also mention the publication [6] where the BENJAMIN-BONA-MAHONY (BBM) equation was considered on a tree. The sG equation on Y -shaped JOSEPHSON junctions was first considered in [30, 31]. The dynamics of kinks in Y -junctions was studied in [17, 21]. However, these studies do not rely on any particular variational structure of the governing equation; the boundary conditions come from a particular tri-layer of superconducting films. The existence and stability of solitary waves ‘sitting’ near the junction point was studied in [36].

In the present study we consider the celebrated sine-GORDON (sG) equation which is a HAMILTONIAN and integrable PDE [11, 37]. However, the integrability of the sG equation is not compulsory for our purposes. In the developments presented below we will use the

HAMILTONIAN and LAGRANGIAN structures to determine the relevant conserved quantities and correct interface conditions at the vertices in order to construct an appropriate symplectic discretization. In the present study, we consider the discrete dynamics of sG on 1–D lattices assembled into a graph. The transition rules between the adjacent lattices at junction points follow from the discretization of the local conservation laws. This approach was already used in [5, 8]. We expect that the limit of the lattice parameter $\Delta \rightarrow 0$ will provide us with the continuous version of the HAMILTONIAN mechanics on non-manifolds.

Our main result is a detailed methodology to solve HAMILTONIAN evolution equations on networks. We give this in full detail and explain which sections can be parallelized. For the case of the sG or another nonlinear HAMILTONIAN equation, we justify the coupling conditions at the vertices of the network using a homothetic approach and conservation laws. Note that this derivation of the coupling conditions will change for another system of equations like the nonlinear shallow water equations. Finally we compute the evolution of kinks and breathers in a particular graph.

The article is organized as follows. In the following Section 2 we present some basic facts on the sG equation and justify the interface conditions. In Section 3, we introduce our detailed methodology to solve HAMILTONIAN evolution equations on networks. We apply it to the sG equation. Numerical solutions for kinks and breathers on a given graph are shown in Section 4 and we discuss these results in Section 5.

2. Continuous sine–Gordon equation

Consider the real space-time coordinates $(x, t) \in \mathbb{R} \times \mathbb{R}^+$. Then, the most common version of the sine–GORDON (sG) equation reads [34]

$$u_{tt} - u_{xx} + \sin u = 0, \quad (2.1)$$

where the subscripts $(\cdot)_t, (\cdot)_x$ denote the derivatives with respect to the time t and space x coordinates. In order to obtain a well-posed boundary value problem, equation (2.1) is completed by periodic or homogeneous NEUMANN boundary conditions. The linear part $\square^2 u \stackrel{\text{def}}{=} u_{tt} - u_{xx}$ is the D’ALEMBERTIAN or LAPLACIAN in MINKOWSKI space \mathbb{M}^2 . The sG equation is known to be LORENTZ invariant and an integrable PDE [14].

2.1. Variational structure

The sG equation can be derived as the EULER–LAGRANGE equation of the following LAGRANGIAN density*

$$\mathcal{L}_{\text{sG}} \stackrel{\text{def}}{=} \frac{1}{2} (u_t^2 - u_x^2) - 1 + \cos u. \quad (2.2)$$

*One can notice that this LAGRANGIAN is classical since it can be seen as the kinetic minus potential energies. See, for example [35].

Moreover, the sG equation possesses also the HAMILTONIAN formulation

$$\mathbf{z}_t = \mathbf{J} \delta_{\mathbf{z}} \mathcal{H}, \quad \mathbf{J} \stackrel{\text{def}}{=} \begin{pmatrix} 0 & 1 \\ -1 & 0 \end{pmatrix}, \quad (2.3)$$

$\mathbf{z} \stackrel{\text{def}}{=}} (u, v)$, $\delta_{\mathbf{z}} \stackrel{\text{def}}{=} (\delta_u, \delta_v)$ is the variational gradient, \mathbf{J} is the symplectic operator and, finally, the HAMILTONIAN functional \mathcal{H} is defined as

$$\mathcal{H}\{\mathbf{z}\} \stackrel{\text{def}}{=} \int_{-\infty}^{+\infty} \left[\frac{1}{2} v^2 + \frac{1}{2} u_x^2 + 1 - \cos u \right] dx.$$

It can be obtained by a LEGENDRE transform. Equations (2.3) can be rewritten component-wise form for the sake of clarity

$$\begin{aligned} u_t &= \frac{\delta \mathcal{H}}{\delta v} = v, \\ v_t &= -\frac{\delta \mathcal{H}}{\delta u} = u_{xx} - \sin u. \end{aligned}$$

Consequently, the sG equation is a HAMILTONIAN system with phase space (u, v) and the symplectic form

$$\omega \stackrel{\text{def}}{=} \int_{-\infty}^{+\infty} du \wedge dv dx. \quad (2.4)$$

The multi-symplectic structure of the sG equation is discussed in [23].

The sG equation has an infinite number of conserved quantities [1]. It is therefore an integrable infinite dimensional HAMILTONIAN system. Among the conserved quantities two are particularly important, the HAMILTONIAN and the momentum. The HAMILTONIAN $\mathcal{H}\{u, v\} \equiv \mathcal{E}\{u\}$ has the sense of the physical energy

$$\mathcal{E}\{u\} \stackrel{\text{def}}{=} \int_{-\infty}^{+\infty} \left[\frac{1}{2} u_t^2 + \frac{1}{2} u_x^2 + 1 - \cos u \right] dx.$$

Remark 1. *There is another important functional conserved for the equation (2.1) which can be associated to the total momentum*

$$\mathcal{M}\{\mathbf{z}\} \stackrel{\text{def}}{=} \int_{-\infty}^{+\infty} u_t u_x dx.$$

The conservation of $\mathcal{M}\{\mathbf{z}\}$ can be readily checked by computing $\frac{d\mathcal{M}}{dt}$.

2.2. Exact solutions

The sG equation has constant solutions*

$$u(x, t) \equiv 2k\pi, \quad (2.5)$$

*After substituting a constant solution ansatz $u(x, t) \equiv C$ into sG equation (2.1) we obtain that necessarily $\sin C = 0$. Thus, $C = l\pi$ with $l \in \mathbb{Z}$. However, only even values of $l = 2k$, $k \in \mathbb{Z}$ correspond to the minima of the potential energy. So, we keep only this sub-family of constant solutions.

where $k \in \mathbb{Z}$ is an integer. These have zero energy and are ground states. A first non trivial (*i.e.* non-constant) solution is the *kink* [35]:

$$u(x, t) = 4 \arctan e^{\gamma(x - x_0 - ct)}, \quad x_0 \in \mathbb{R}, \quad (2.6)$$

where $c \in [0, 1)$ is the kink celerity and γ is the so-called LORENTZ factor

$$\gamma^2 \stackrel{\text{def}}{=} \frac{1}{1 - c^2}. \quad (2.7)$$

The energy of the kink can be computed analytically, $\mathcal{E} = 8\gamma$. In our scaling the speed of light is equal to 1. The kink solution realizes a smooth transition between the two ground states $0 \rightsquigarrow 2\pi$. More generally, kinks link in phase space two neighbouring states $2\pi k \rightsquigarrow 2\pi(k \pm 1)$.

There is also another type of exact solutions to the sG equation — the *breathers* [1]. These solutions are localized and oscillate in space and in time; their analytical expression is given by [39]:

$$u(x, t) = 4 \arctan \left\{ \tan \mu \frac{\cos(\omega \gamma (t + x_0 c - x c))}{\cosh(\sin \mu \cdot \gamma (x - x_0 - ct))} \right\}, \quad x_0 \in \mathbb{R},$$

where the parameter μ is defined through the relation $\cos \mu \equiv \omega$. The energy of a breather depends both on its speed and frequency as:

$$\mathcal{E} = 16\gamma \sqrt{1 - \omega^2}.$$

2.3. Coupling conditions at the junctions

We now consider that the sG equation is defined on each branch E of an oriented network $G = (V, E)$ where V is a set of vertices and E the set of branches. We label the branches $m = 1, \dots, |E|$. To fix the notations, consider a Y -junction composed of three semi-infinite rays $\mathcal{S}_{1,2,3}$ embedded into the EUCLIDEAN space \mathbb{R}^2 :

$$\mathcal{Y} \stackrel{\text{def}}{=} \left\{ \mathbf{x} \in \mathbb{R}^2 : \exists i \in \{1, 2, 3\} \text{ such that } \mathbf{x} \in \mathcal{S}_i \right\}.$$

The intersection of all three strings is located at the unique point $C \in \mathbb{R}^2$ defined as (see Figure 2 for the illustration):

$$C \stackrel{\text{def}}{=} \mathcal{S}_1 \cap \mathcal{S}_2 \cap \mathcal{S}_3.$$

Henceforth, each ray \mathcal{S}_i starts at the junction point C and continues, for the sake of simplicity, indefinitely in the prescribed direction*. A simple topological argument can be applied to show that the set \mathcal{Y} is not homeomorphic to any EUCLIDEAN space. Indeed, let us remove virtually the junction point C from this set \mathcal{Y} . It will be decomposed in three disjoint components. Clearly, any EUCLIDEAN space \mathbb{R}^n , $n \geq 1$ does not have such a point with the same property.

*Of course, this idealization is adopted only for the problem formulation. In our numerical simulations we assume the branches \mathcal{S}_i to be finite with length ℓ_i .

A first natural condition to be satisfied at the junction point C is the continuity of the solution

$$\lim_{x \rightarrow C, x \in \mathcal{S}_1} u(x, t) = \lim_{x \rightarrow C, x \in \mathcal{S}_2} u(x, t) = \lim_{x \rightarrow C, x \in \mathcal{S}_3} u(x, t). \quad (2.8)$$

Moreover, this condition has to be completed by the “charge” conservation property adopted in previous studies of the KLEIN–GORDON [5, 28] and sG [8] equations:

$$\partial_1 u|_{x \rightarrow C, x \in \mathcal{S}_1} + \partial_2 u|_{x \rightarrow C, x \in \mathcal{S}_2} + \partial_3 u|_{x \rightarrow C, x \in \mathcal{S}_3} = 0, \quad (2.9)$$

where ∂_i denotes the first spatial derivative along the branch \mathcal{S}_i , $i = 1, 2, 3$. Condition (2.9) is a continuous analogue of the celebrated KIRCHHOFF’s circuit law. We will justify these conditions in the next two sections using an homothetic argument and conservation laws respectively.

Before justifying the coupling conditions, let us examine the structure of the phase space associated to the sG dynamics on our Y –junction, *i.e.* the center of Figure 4. The augmented phase space of the sG equation restricted to a branch (say e_1) consists in $\mathcal{P} \times \mathcal{A}$, where $\mathcal{P} \stackrel{\text{def}}{=} (u_{tt}, u_t, u, u_x, u_{xx})$ is the usual configuration space and \mathcal{A} is the spatial extent of a branch ($\mathcal{A} = [v_1, v_2]$ in this particular case). We have to augment the configuration space \mathcal{P} by \mathcal{A} since the joints are realized on the boundaries of the interval \mathcal{A} . This portion of the phase space is schematically represented on Figure 1 for the Y –junction; in Geometry these structures are called *foliations* [20]. This is only the local structure of the global phase space; to represent the global phase space associated to a network, the borders of the phase spaces of the individual branches, the leaves on Figure 1, would have to be glued together in accordance with the scheme prescribed by the graph G .

2.3.1 Back-to-Manifold: a homothetic approach

Condition (2.9) can be justified by converting (‘*inflating*’) the Y –junction domain into a manifold \mathcal{Y}_δ of small thickness $\delta > 0$. Thus, \mathcal{Y}_δ becomes a tubular neighbourhood* of our network. Moreover, the two-dimensional version of the sG equation becomes

$$u_{tt} - \nabla^2 u + \sin u = 0. \quad (2.10)$$

The elements necessary to the proof are shown on Figure 3. On the boundary $\partial\mathcal{Y}_\delta$ we impose the homogeneous NEUMANN condition [8, 18]:

$$\partial_n u|_{x \in \partial\mathcal{Y}_\delta} = 0, \quad \partial_n u \stackrel{\text{def}}{=} \nabla u \cdot \mathbf{n}, \quad (2.11)$$

*This tubular neighbourhood should be considered as a surface.

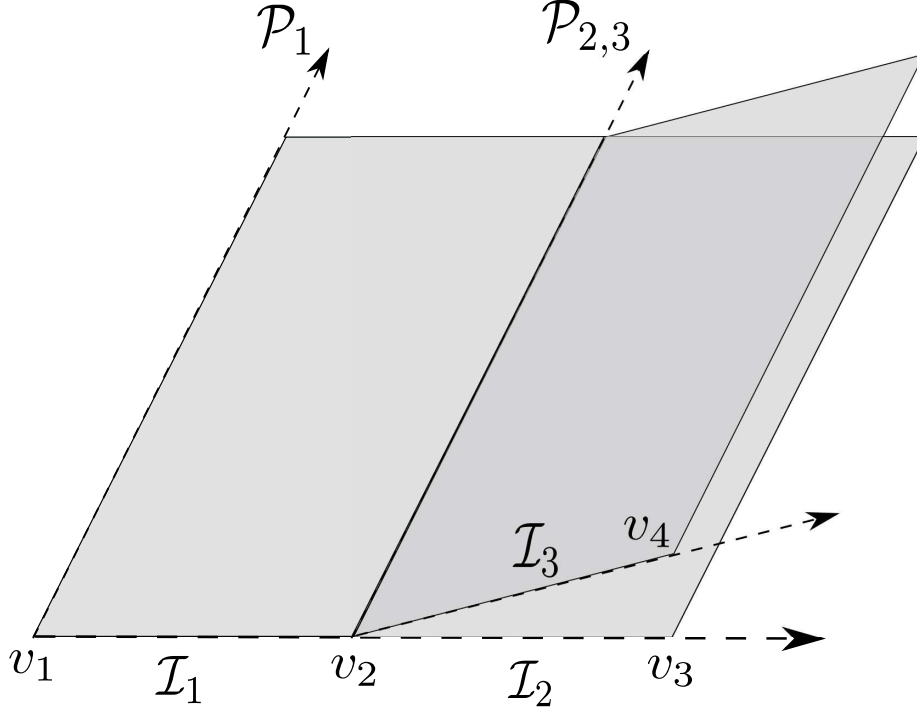


Figure 1. A schematic representation of the foliation of the phase spaces at a junction point.

To justify (2.9) we integrate the 2D version of the sG equation 2.10 over the domain $\Omega_\delta \cap \mathcal{Y}_\delta^*$ and use the STOKES theorem for the divergence (LAPLACIAN) term:

$$\iint_{\Omega_\delta \cap \mathcal{Y}_\delta} [u_{tt} - \nabla^2 u + \sin u] d\mathbf{x} = \underbrace{\iint_{\Omega_\delta \cap \mathcal{Y}_\delta} [u_{tt} + \sin u] d\mathbf{x}}_{(i)} + \underbrace{\int_{\partial(\Omega_\delta \cap \mathcal{Y}_\delta)} \partial_n u ds}_{(ii)} = 0.$$

Assuming the solution $u(\mathbf{x}, t)$ to be smooth and bounded in Ω_δ , the first integral (i) scales as $\mathcal{O}(\delta^2)$. Taking into account the boundary condition (2.11), the second integral (ii) becomes just the sum of three line integrals over ℓ_i in the interior of the domain \mathcal{Y}_δ (represented in red on Figure 3). Thus the sum of the two integrals reduces to

$$\mathcal{O}(\delta^2) + \sum_{i=1}^3 \underbrace{\int_{\ell_i} \partial_n u ds}_{\mathcal{O}(\delta)} = 0,$$

where under the same assumptions on the solution $u(x, t)$, the integrals in the second sum scale as $\mathcal{O}(\delta)$. Thus, dividing the identity by δ and taking the limit $\delta \rightarrow 0$, we obtain

*The domain $\Omega_\delta \stackrel{\text{def}}{=} \mathcal{D}_{2\delta}(C)$ is the disc of radius 2δ centered at the junction point C depicted on Figure 3.

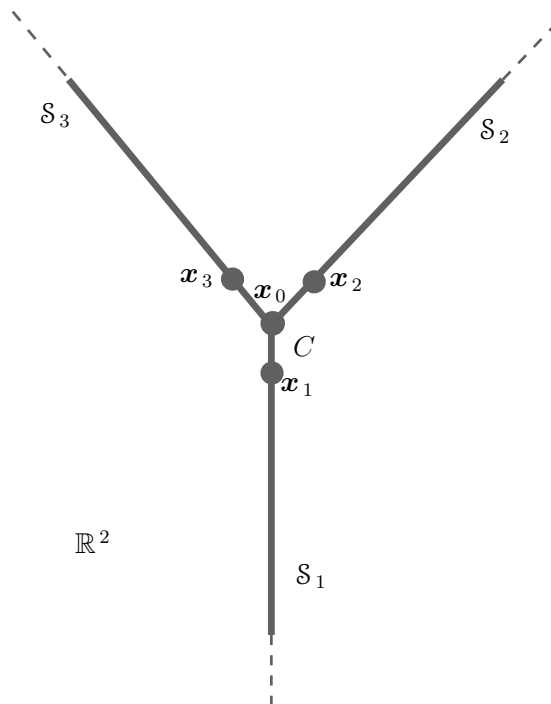


Figure 2. Sketch of a Y -junction composed of three strings $\mathcal{S}_{1,2,3}$ with the center located at the point C .

the desired result (2.9). An alternative derivation based on the variational structure can be found in Appendix A.

2.3.2 Conservation laws approach

Energy. The main conserved quantity, the energy can be used to justify the interface conditions (2.9). The energy of a network is

$$\mathcal{E} = \sum_{i=1}^m \int_{a_i}^{b_i} \left[\frac{1}{2}(u_t^2 + u_x^2) + 1 - \cos u \right] dx, \quad \ell_i \stackrel{\text{def}}{=} b_i - a_i,$$

where the sum is taken over all m branches of the network and the branch i starts from the node a_i and finishes at the node b_i . Taking the time derivative of \mathcal{E} we get

$$\frac{d\mathcal{E}}{dt} = \sum_{i=1}^m [u_t u_x]_{a_i}^{b_i}.$$

We can assume that the nodes a_i and b_i are uncoupled. This is natural since information can only travel from a_i to b_i at a finite speed. Therefore, to satisfy $\frac{d\mathcal{E}}{dt} = 0$ we need that

$$\sum_i u_t u_x|_{a_i} = \sum_i u_t u_x|_{b_i} \equiv 0.$$

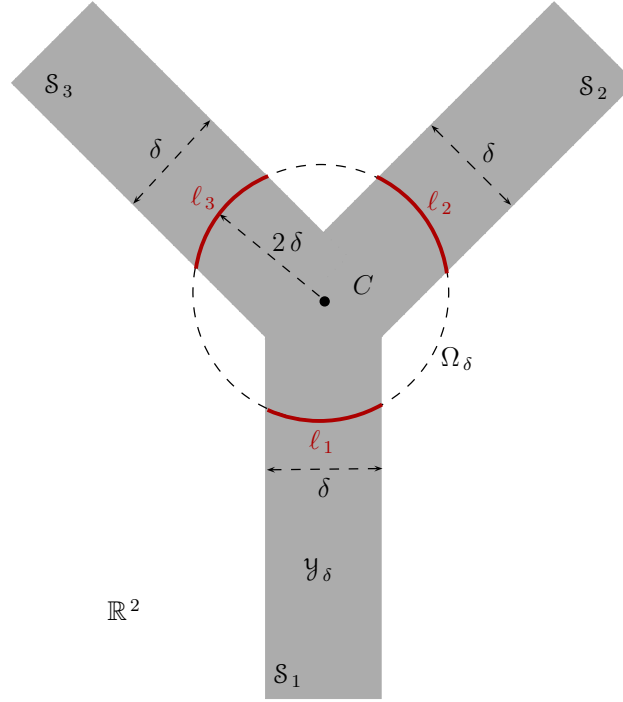


Figure 3. The Y -junction from the previous Figure 2 converted into a manifold \mathcal{Y}_δ by extending all the branches to some finite thickness $\delta > 0$.

For a Y -junction, this can be satisfied if u_t is continuous, *i.e.* $u_{1t} = u_{2t} = u_{3t}$ and $-u_{1x} + u_{2x} + u_{3x} = 0$, which is precisely the KIRCHOFF law (2.9).

These coupling conditions (2.8) and (2.9) are natural in terms of the electrodynamics of JOSEPHSON junctions where the variable u is the phase difference between the two superconductors and where u_x is the surface current in the junction. The conditions (2.8) and (2.9) state that the phase is continuous and that the currents satisfy KIRCHOFF's law.

Momentum. One could try to impose similarly the conservation of the total momentum of the network:

$$\mathcal{M} = \sum_{i=1}^m \int_{a_i}^{b_i} u_t u_x \, dx.$$

We can compute $\frac{d\mathcal{M}}{dt}$, impose momentum conservation condition $\frac{d\mathcal{M}}{dt} = 0$ and follow the same procedure as above and obtain

$$\sum_{i=1}^m \left[\frac{1}{2}(u_t^2 + u_x^2) - 1 + \cos \mathbf{u} \right]_{a_i} = \sum_{i=1}^m \left[\frac{1}{2}(u_t^2 + u_x^2) - 1 + \cos \mathbf{u} \right]_{b_i}.$$

We then get for the Y -junction, taking into account (2.8) and (2.9):

$$-u_{1x}^2 + u_{2x}^2 + u_{3x}^2 = 0,$$

which cannot be satisfied in general. This problem exists also for the shallow water equations in a junction [9]. We then see that on a network we lose a number of conserved quantities.

In the sequel of the paper we require continuity (2.8) and ‘charge’ conservation (2.9) at the junction points. We also remark the following:

- This approach can be generalized to any general nonlinearity in equation (2.1), not only $f(u) = \sin u$:

$$u_{tt} - u_{xx} + f(u) = 0.$$

- This approach can also be applied to non-HAMILTONIAN systems. There one should consider other conservation laws, see for example the nonlinear shallow water equations [9].
- The compatibility conditions (2.8), (2.9) at the graph vertices can be straightforwardly generalized to situations where any (finite) number of strings meet at one junction point. Another generalization consists in assigning different weights ω_i , $i = 1, 2, 3, \dots$ to incident edges. They can be interpreted as widths of channels, for example. The derivation of coupling conditions in this case can be found *e.g.* in [8].
- It goes without saying that the initial condition $u(\mathbf{x}, t = 0) = u_0(\mathbf{x})$ on a graph G should satisfy conditions (2.8) and (2.9).

3. Numerical implementation : the discrete sine-Gordon equation

Traditionally, the sG equation was solved numerically among others using finite difference [15], finite element [3, 8], tension spline [32] and radial basis functions [12, 22] methods. In order to propose a discrete version of the sG equation we will follow the variational framework. Recall that the sG equation is a HAMILTONIAN PDE. A natural way to convert it into a discrete dynamical system is to employ a symplectic discretization [25]. The workflow is determined by the method of lines:

- Discretize the HAMILTONIAN functional $\mathcal{H}[\mathbf{z}]$ in space on a lattice to obtain a system of coupled HAMILTONIAN ODEs
- Discretization in time the system of HAMILTONIAN ODEs using a symplectic scheme.

This programme will be realized below by following the main lines of [25]. Please, notice also the differences between symplectic and variational integrators [26, 27].

Consider a uniform lattice $\{x_j = k\Delta x \mid j = 1, \dots, n\}$, $\Delta x > 0$. The values of the sG solution $u(x, t)$ at lattice points will be denoted by $u_j \approx u(x_j)$. For the moment we will consider only interior nodes. The junction points (end points of the lattice) will be discussed below. After the discretization, the phase space becomes finite dimensional, since $\{\mathbf{z}_j\}_{j=1}^n = \{(u_j, v_j) \in \mathbb{R}^2\}_{j=1}^n \in \mathbb{R}^{2n}$. The discrete symplectic form on this

space becomes

$$\omega_n = \sum_{j=1}^n du_j \wedge dv_j \Delta x,$$

which is a straightforward discretization of (2.4). The HAMILTONIAN functional will be approximated with the *rectangular rule* as the following sum

$$\mathcal{H}_n[\{u_j, v_j\}] = \sum_{j=1}^n \left[\frac{1}{2} v_j^2 + \frac{1}{2} \left(\frac{u_j - u_{j-1}}{\Delta x} \right)^2 + 1 - \cos u_j \right] \Delta x.$$

The system of HAMILTONIAN ODEs follows automatically

$$\frac{dz_j}{dt} = \mathbf{J}_n \cdot \nabla_{z_j} \mathcal{H}_n[\mathbf{z}], \quad \mathbf{J}_n = \begin{pmatrix} \mathbf{0} & \mathbb{I}_n \\ -\mathbb{I}_n & \mathbf{0} \end{pmatrix}, \quad i = 1, \dots, n.$$

After computing the derivatives, the last semi-discrete system becomes

$$\frac{du_j}{dt} = v_j, \quad (3.1)$$

$$\frac{dv_j}{dt} = \frac{w_{j+1} - w_j}{\Delta x} - \sin u_j, \quad (3.2)$$

where $w_{j+1}(t) \stackrel{\text{def}}{=} \frac{u_{j+1} - u_j}{\Delta x}$ and $w_j(t) \stackrel{\text{def}}{=} \frac{u_j - u_{j-1}}{\Delta x}$. It can be shown [25] that the semi-discrete scheme (3.1), (3.2) satisfies a local energy conservation law

$$\frac{d}{dt} \left[\frac{1}{2} v_j^2 + \frac{1}{2} w_j^2 + 1 - \cos u_j \right] + \frac{F_{j+\frac{1}{2}} - F_{j-\frac{1}{2}}}{\Delta x} = 0, \quad (3.3)$$

where the quantity in brackets $\mathcal{E}_j \stackrel{\text{def}}{=} \frac{1}{2} v_j^2 + \frac{1}{2} w_j^2 + 1 - \cos u_j$ is the (semi-)discrete energy and $F_{j+\frac{1}{2}} \stackrel{\text{def}}{=} -v_j w_{j+1}$, $F_{j-\frac{1}{2}} \stackrel{\text{def}}{=} -v_{j-1} w_j$ are the energy fluxes.

In order to obtain a fully discrete scheme, the system of ODEs (3.1), (3.2) can be discretized in time with a *symplectic Euler* method, for example:

$$\begin{aligned} u_j^{m+1} &= u_j^m + \Delta t v_j^{m+1}, \\ v_j^{m+1} &= v_j^m + \Delta t \left[\frac{w_{j+1}^m - w_j^m}{\Delta x} - \sin u_j^m \right], \end{aligned}$$

where $\Delta t > 0$ and $u_j^m \stackrel{\text{def}}{=} u(x_j, t_m)$, $t_m \stackrel{\text{def}}{=} m \Delta t$, $m = 1, 2, \dots$. After eliminating v_j^n and w_j^n from these equations we obtain the classical leap-frog scheme as a fully discrete analog of the sG equation

$$\frac{u_j^{m+1} - 2u_j^m + u_j^{m-1}}{\Delta t^2} - \frac{u_{j+1}^m - 2u_j^m + u_{j-1}^m}{\Delta x^2} + \sin u_j^m = 0.$$

After simple algebraic manipulations we can obtain the following discrete dynamical system for the interior nodes of the lattice:

$$u_j^{m+1} = 2u_j^m - u_j^{m-1} + \left(\frac{\Delta t}{\Delta x}\right)^2 \underbrace{\left[u_{j+1}^m - 2u_j^m + u_{j-1}^m\right]}_{\stackrel{\text{def}}{=} \mathcal{L} u^m} - \Delta t^2 \sin u_j^m, \quad m = 1, 2, \dots, \quad (3.4)$$

where for the sake of simplicity we introduced the linear operator \mathcal{L} , which represents the discretization of the classical LAPLACE operator. The treatment of nodes at junctions will be discussed below in Sections 3.2 and 3.3. We underline that our discretization being explicit is subject to a CFL-type condition on the time step [10]. However, this restriction is of hyperbolic type, which is quite gentle, and we had no practical difficulties to satisfy it.

In general, one cannot expect to have the fully discrete energy conservation law similar to (3.3), in contrast to the semi-discrete schemes. The reason is that a symplectic scheme aims to preserve the symplectic form and it does not guarantee anything about the HAMILTONIAN. However, the backward error analysis explains why, in general, the symplectic discretizations of PDEs show satisfactory energy conservation properties [29].

3.1. Formulation on graphs

In this Section we will describe the assembling procedure of 1D lattices $\ell_i \stackrel{\text{def}}{=} \{\mathbf{x}_j \in [\mathbf{a}_i = \mathbf{x}_1, \mathbf{b}_i = \mathbf{x}_{n_i}] | j = 1, \dots, n_i\}$ into a network whose mathematical description is usually given on the language of the graph theory. In the sequel we will denote by $\mathbf{a}_i, \mathbf{b}_i$ the starting and terminal points of the lattice ℓ_i respectively.

Consider a simple oriented network-shaped weighted graph $G := (V, E)$. The finite set of vertices V is basically the union of lattice initial and terminal nodes:

$$V \stackrel{\text{def}}{=} \{\mathbf{v}_j\}_{j=1}^m \equiv \bigcup_{i=1}^{|E|} \{\mathbf{a}_i, \mathbf{b}_i\}.$$

The finite set of edges $E \subseteq \{(\mathbf{a}, \mathbf{b}) \in V^2 | \mathbf{a} \neq \mathbf{b}\}$. Every edge $e_i \stackrel{\text{def}}{=} (\ell_i, \omega_i)$ consists of 1D lattice segments whose orientation is naturally determined by the enumeration of discrete lattice points (or equivalently the choice of the first and last points \mathbf{a}_i and \mathbf{b}_i). The *length* of the edge ℓ_i can be prescribed through its weight ω_i :

$$\omega_i \stackrel{\text{def}}{=} |\ell_i| \Delta x_i \equiv n_i, \quad i = 1, \dots, |E|.$$

where $|\ell_i|$ is the number of points in the lattice and Δx_i is the spacing between two consecutive points.

The internal organization of the network G is traditionally given by graph-theoretical data structures such as the incidence and adjacency matrices [16]. In the present study

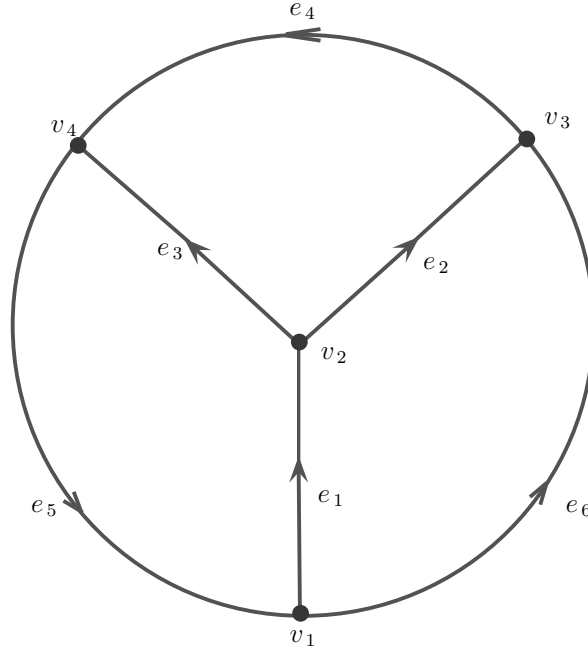


Figure 4. A sample graph used in our study for the sake of illustration.

we will privilege the incidence matrix representation. By definition, the incidence matrix $A = (A_{ij})_{n \times m} \in \text{Mat}_{n_e \times m}(\mathbb{Z})$, $n \stackrel{\text{def}}{=} |V|$, $m \stackrel{\text{def}}{=} |E|$ has the following elements:

$$A_{ij} = \begin{cases} +1, & \text{if the edge } e_j \text{ enters the vertex } v_i, \\ -1, & \text{if the edge } e_j \text{ leaves the vertex } v_i, \\ 0, & \text{otherwise.} \end{cases}$$

The edges are considered to be directional. For the sake of illustration let us consider the graph $G_0 = (V, E)$ represented on Figure 4. It is composed of four vertices $V = \{v_1, v_2, v_3, v_4\}$ and six edges $E = \{e_1, \dots, e_6\}$. It is straightforward to check that the incidence matrix \mathcal{A}_0 of the graph G_0 is

$$\mathcal{A}_0 = \begin{pmatrix} -1 & 0 & 0 & 0 & 1 & -1 \\ 1 & -1 & -1 & 0 & 0 & 0 \\ 0 & 1 & 0 & -1 & 0 & 1 \\ 0 & 0 & 1 & 1 & -1 & 0 \end{pmatrix}.$$

However, the most important information for us is the correspondence between the vertices v_i with starting/terminal points of the lattices which compose the edges e_j . This correspondence is given as a list:

$$\begin{aligned} v_1 &= \{\mathbf{a}_1, \mathbf{a}_6, \mathbf{b}_5\}, & v_3 &= \{\mathbf{a}_4, \mathbf{b}_2, \mathbf{b}_6\}, \\ v_2 &= \{\mathbf{a}_2, \mathbf{a}_3, \mathbf{b}_1\}, & v_4 &= \{\mathbf{a}_5, \mathbf{b}_3, \mathbf{b}_4\}. \end{aligned}$$

3.2. Conditions on junctions: the discrete case

It is straightforward to obtain the discrete version of compatibility conditions (2.8), (2.9) by following the approach proposed in [8]. By using the continuity condition (2.8), we can employ for simplicity the forward finite differences written on adjacent nodes (see Figure 2 for the illustration). Let us denote the values of the solution at neighbouring points \mathbf{x}_i , $i = 0, \dots, 3$ as $u_i \stackrel{\text{def}}{=} u(\mathbf{x}_i)$. Then, the discrete compatibility condition reads:

$$\frac{u_1 - u_0}{\Delta x} + \frac{u_2 - u_0}{\Delta x} + \frac{u_3 - u_0}{\Delta x} = 0 \quad \Rightarrow \quad u_0 = \frac{1}{3}(u_1 + u_2 + u_3). \quad (3.5)$$

Obviously, as in the continuous case, the last discrete condition can be generalized to any finite number of adjacent strings.

3.3. The numerical algorithm

Taking into account all the information given above, we have all the elements to describe a practical implementation of the numerical algorithm. Each edge $e_i \in E$ is discretized with n equally spaced points. We have in total $m = |E|$ edges. Thus, it seems natural to keep the discrete solution using three matrices $U_0, U_1, U_2 \in \text{Mat}_{n \times m}(\mathbb{R})$. The upper index $k \in \mathbb{N}_0$ indicates the time step number, *i.e.* the initial condition is discretized into U_0 and U_1 . Please, note that the number of initial (or boundary) conditions in the continuous and discrete formulations might not coincide (see [24, Appendix A] for more details). In our problem two initial conditions are required by the continuous sG equation and two initial conditions are needed by the fully discrete scheme (3.4). In the present study we choose U_0, U_1 to be a perfect coherent structure (*i.e.* kink or breather) propagating in the required direction. The pseudo-code for the discrete time evolution U_k , $k \geq 2$ is given in Algorithm 1. We first advance the bulk of the edges and then update the graph vertices where several edges begin or end. The update is done using condition (3.5). A vertex is associated to $U_k(1, j)$ if branch j is out-going from it and $U_k(n, j)$ if branch j is entering it. The source code, implemented in the MATLAB environment is freely available to consult and download at the following URL:

<https://github.com/dutykh/sineGordonGraph/>

Algorithm 1 Algorithm to simulate a HAMILTONIAN equation, like the sine-GORDON (sG) equation on a network. Here n_d is the degree of each vertex in the graph G . This parameter is different from n , the number of discretization points of graph edges.

Require: $d(n_d)$ ▷ Degree of each node
Require: $\text{In}(n_d), \text{Out}(n_d)$ ▷ Input and output branches of each node
Require: $U_0(n, m)$ and $U_1(n, m)$ ▷ Initial conditions
1: $t \leftarrow 0$ ▷ We start the simulation at $t = 0$
2: **while** $t < T_f$ **do** ▷ T_f is the final simulation time and t is the current time
3: **for** $j \leftarrow 1, m$ **do** ▷ Loop over the edges
4: $U_2(2:n-1, j) \leftarrow 2U_1(2:n-1, j) - U_0(2:n-1, j) + \left(\frac{\Delta t}{\Delta x}\right)^2 \mathcal{L} \cdot U_1(2:n-1, j) - \Delta t^2 \sin U_1(2:n-1, j)$ ▷ Update the solution in bulk of edges
5: **end for**
6: **for** $\text{in} \leftarrow 1, n_d$ **do** ▷ Loop over the vertices
7: $V \leftarrow (\sum(U_2(n-1, \text{In}(\text{in}))) + \sum(U_2(n-1, \text{Out}(\text{in}))))/d(\text{in})$ ▷ Condition (3.5)
8: $U_2(n, \text{In}(\text{in})) \leftarrow V; U_2(1, \text{Out}(\text{in})) \leftarrow V$ ▷ Update edges of branches
9: **end for**
10: $U_0(:, :) \leftarrow U_1(:, :)$
11: $U_1(:, :) \leftarrow U_2(:, :)$
12: $t \leftarrow t + \Delta t$ ▷ Update the time variable
13: **end while** ▷ End of main loop in time

Note that the ‘bulk’ advances in the edges, steps 3, 4 and 5 can be done in parallel. Then threads need to be synchronized for the vertex update. In order to represent graphically the solution, one has to specify also an embedding of the graph G on \mathbb{R}^2 (for planar graphs and \mathbb{R}^3 in the general case), *i.e.* a family of regular maps $g_i : e_i \in E \mapsto \mathbb{R}^2$ which satisfy the natural compatibility conditions at the vertices. For the graph G_0 we chose a natural embedding shown on Figure 5.

4. Numerical results

Below we present several applications of the proposed numerical scheme on a particular graph. As illustrations, we present the propagation of two coherent structures (kinks and breathers) over this graph.

4.1. Propagation of kinks

The initial condition consists of three kinks (2.6) with velocity $c = 0.95$ initially placed on the edges e_1, e_5, e_6 propagating vertically upwards and connecting 0 to 2π . Solution

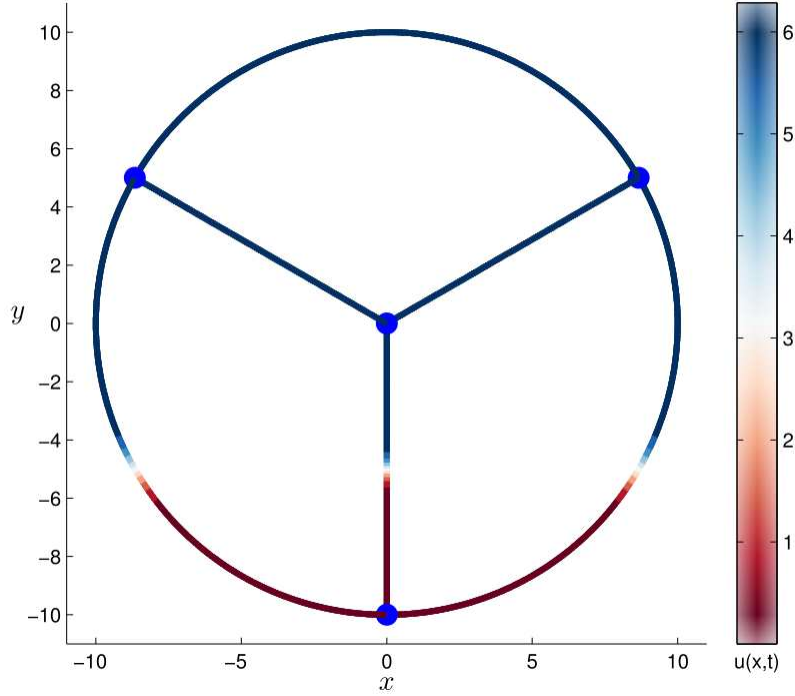


Figure 5. Embedding of the graph G_0 in the plane \mathbb{R}^2 along with the initial condition (represented with the color of the edges E) for three kinks propagating upwards in the network. Graph vertices V are represented with bold blue points.

values on other edges are chosen in order to satisfy the continuity condition (2.8). The values of all numerical parameters are given in Table 1. The total energy of this system is equal to

$$\mathcal{E}(0) = 3 \times 8\gamma \approx 76.86151382644181,$$

where γ is defined in (2.7). For the sake of comparison, the energy at the end of the simulation was equal to $\mathcal{E}(T) \approx 76.97$, which shows good conservative properties of the scheme (the relative error is less than 1.5%).

The evolution of this initial condition on the interval $[0, T]$ under the sG dynamics is shown on Figure 6. When the kinks arrive at vertices v_2 , v_3 and v_4 (see Figure 6(a)) they split in six kinks (see Figure 6(b)), which collide again right in the middle of the edges e_2 , e_3 and e_4 . We observe a topological change at the moment of the collision (see Figure 6(c, d)), since all the kinks switch from the ground state $0 \rightsquigarrow 2\pi$ to $0 \rightsquigarrow -2\pi$ as a result of the mutual reflection. Then, the newly generated kinks propagate vertically downwards along the graph edges e_1 , e_5 and e_6 (see Figure 6(e)). Finally, at the end of the simulation the three kinks collide again in the vicinity of the vertex v_1 . At the moment of collision there is another topological change from $0 \rightsquigarrow -2\pi$ to $-2\pi \rightsquigarrow -4\pi$ (which are constant admissible solutions (2.5)). We would like to mention that we observe the generation of a small reflected wavelet into the incident branch when a kink arrives to a junction. However, we do not exclude a possibility that this wavelet might be a

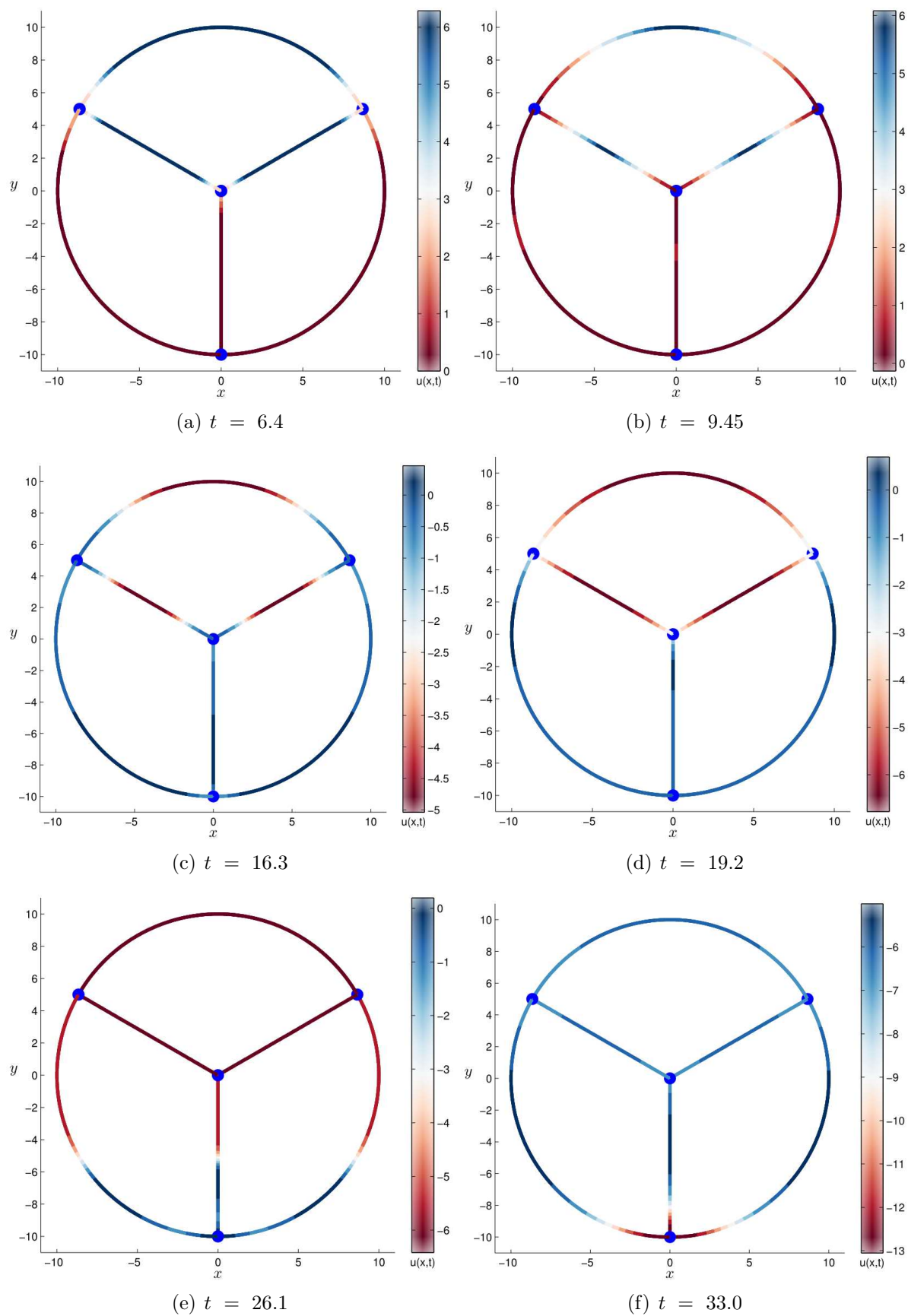


Figure 6. Evolution of three *sG* kinks (with $c = 0.95$) on the graph G_0 .

<i>Parameter</i>	<i>Value</i>
Kink speed, c_0	0.95; 0.5
Time step, Δt	0.01
Final simulation time, T	33.0; 40.0
Number of time steps, N_t	4 000
Number of points, N	500
Spatial discretization step, Δx	0.02

Table 1. *Parameters used in numerical simulations presented in this manuscript. The kink speeds are chosen in order to illustrate the phenomena of transition/reflection through/at the junction. The number of time steps is chosen to have sufficient accuracy by verifying the stability conditions.*

numerical artifact due to discretization and/or the implementation of junction conditions. The corresponding video illustration of this simulation can be watched at this URL:

http://youtu.be/rwZ4d_T7nTs

Let us perform another simulation, where we take the same set-up as described above, but the kinks are initialized to have the speed $c = 0.5$. The dynamics of this initial condition is shown on Figure 7. In agreement with previous investigations (limited to only a single junction) [8, 19] this kink does not possess enough energy to go through a junction. Consequently, the dynamics is confined only to the subgraph whose edges were initialized with kinks. Here again we observe a similar phenomenon to the previous case. When the kinks collide at the vertex v_1 (around $t = 30$), there is a topological change and all three solutions shift from $0 \rightsquigarrow 2\pi$ to $2\pi \rightsquigarrow 4\pi$. The corresponding video illustration can be watched at this URL:

<http://youtu.be/CtglMe0IcBk>

The presented simulations allow us to draw already some conclusions. First of all, there are two distinct situations depending on the kink energy. If this energy is sub-critical, the kinks will be confined to oscillate forever in a small part of the network where they were placed initially. The other situation with super-critical energy is much richer in terms of the generated dynamics. It seems that this dynamics will depend on the network topology. In our study we made a choice for a closed network. As a result, we observe a quasi-periodic dynamics as illustrated in Figure 6.

4.2. Propagation of a breather

The propagation of kinks in simple junctions is becoming a relatively studied topic [8, 18, 21]. In our study we make a further step towards numerical simulations on general

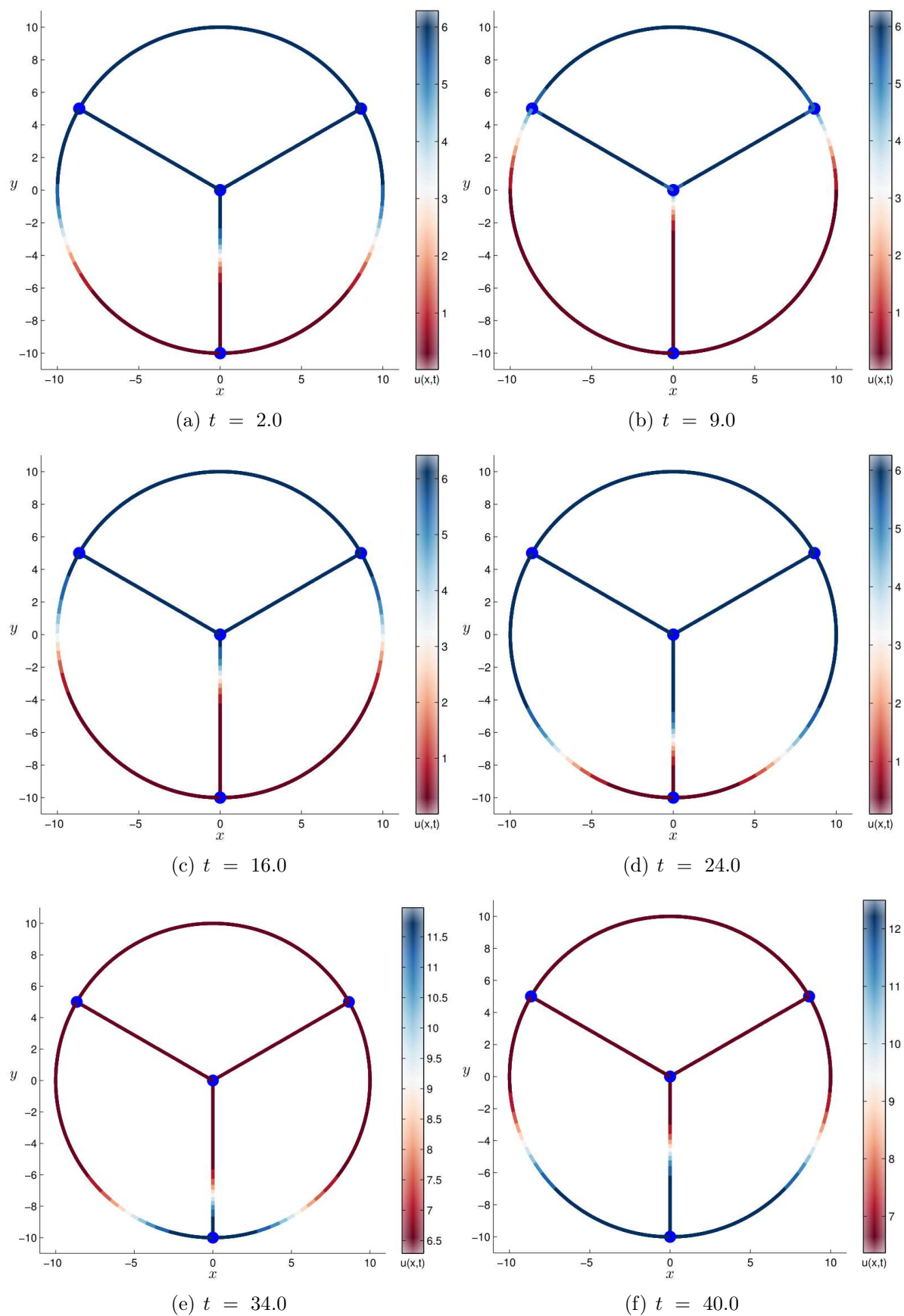


Figure 7. Evolution of three sG kinks (with $c_0 = 0.5$) on the graph G_0 .

networks, which contain numerous junctions. Moreover, our methodology is not limited only to kinks. To illustrate the performance of our algorithm with more general initial conditions, we complete our study with a test case of breather propagation over the same network, which is depicted in Figure 4. The numerical (discretization) parameters and the graph embedding are taken the same as above (see Table 1). The breather has the initial speed $c_0 = 0.95$ and the frequency $\omega = \cos(\frac{\pi}{4}) \equiv \frac{\sqrt{2}}{2}$. Thus, the parameter $\mu = \frac{\pi}{4}$. The energy of this breather is equal to

$$\mathcal{E}(0) = 16\gamma \sin(\mu) \approx 36.23286509262705.$$

Initially the breather is located at the edge e_1 and travels towards the junction point v_2 (see Figure 4). The breather energy is conserved within 1% relative accuracy along the simulation ($t \in [0, T]$, $T = 33.0$) and the total energy evolution has no trend (there are mainly oscillations around the mean level). The evolution of this breather is shown* in Figure 8. The video of this process can be visualized also at this URL address:

<https://youtu.be/doKNMr0kr0o>

From this numerical simulation we can draw the following *preliminary* conclusions on breather dynamics on networks:

- A breather passing through a Y -junction point is partly reflected (see Figure 8(b)). However, most of the energy is transmitted and two newly generated breathers seem to change the polarity, *i.e.* the amplitude changes the sign. As a result, we obtain three breathers (see Figure 8(c)). This property to conserve the type of the coherent structure through the junction should be reminiscent of the integrability of the sG equation
- The same happens at every junction crossing event: a partial reflection[†] and the generation of two new breathers (see Figure 8(d))
- There are important differences with the propagation of kinks. Namely, the kinks pass a junction point without reflecting a breather back into the incident branch. This point is fundamental and it explains why the dynamics of kinks is easier to understand than the dynamics of a single breather in a closed network
- Thus, even if we start with one breather, the dynamics on a closed network becomes rapidly very complicated since the number of coherent structures might increase exponentially (*i.e.* each crossing generates two new breathers, see Figures 8(e, f))
- While propagating in branches, the breathers interact with each other *elastically*[‡], since the sG equation is integrable [11, 37]
- If we had an infinite resolution, we would probably observe something similar to solitonic turbulence in KORTEWEG–DE VRIES-like models [13, 40]

*We change the view angle in order to illustrate better the breather evolution.

[†]The reflected wave is a breather as well of the same polarity.

[‡]The term ‘elastic’ means that coherent structures recover their initial shape after the interaction in contrast to ‘inelastic’ collisions. The property of elasticity in interactions remains rather exceptional since integrable models are exceptional in the world of PDEs.

- However, the system being conservative, the total energy is constant. Thus, the amplitude of breathers can only decrease taking into account the exponential growth of their number. As a result, we deal with decreasingly smaller objects.

To conclude this Section, it would be extremely interesting to study the long time dynamics of such systems, which would require infinite numerical resolutions to capture smaller and smaller coherent structures. Thus, it has to be done theoretically and analytically in future investigations.

4.2.1 Weak energy breather evolution

As a final test case, we consider the evolution of a breather (on the same network) with the energy below the passage barrier. The initial condition is conceptually the same as in the previous Section 4.2, with different numerical parameters, which are given in Table 2. Notice, that we had to take slightly longer branches to put this breather entirely into the edge e_1 . The mesh was refined accordingly to keep approximatively the same level of accuracy. The energy of the ‘weak’ breather is equal to

$$\mathcal{E}(0) = 16\gamma \sin(\mu) \approx 11.68474789344354.$$

This energy was conserved with the relative accuracy $< 1\%$ in our simulation. The evolution of this initial ‘weak’ energy breather is shown in Figure 9. One can see that the breather remains confined forever to the edge e_1 as expected. It is interesting to note that the breather ‘sticks’ somehow to the junction point v_2 and oscillates with it. The breather is apparently never reflected by the junction. All other nodes remain unaffected. The complete video of this process can be visualized also at this URL address:

<https://youtu.be/sncYZU-cbkY/>

5. Conclusions and perspectives

We considered a discrete formulation of a scalar HAMILTONIAN equation on domains which are not manifolds and applied it to the sG equation. More precisely, the 1D lattices are assembled into arbitrary graphs (networks) and the coupled dynamics can be efficiently simulated using our methodology based on a simple symplectic numerical scheme. The edges of the graph deserve a special treatment based on local conservation laws. The performance of this formulation is illustrated on a connected graph involving four cycles. Our computational methodology can easily be generalized to the case where edges or vertices are active as for many engineering applications like fluid or traffic networks. The MATLAB source code, which implements the algorithms described in this study can be freely accessed at the following URL address:

<https://github.com/dutykh/sineGordonGraph/>

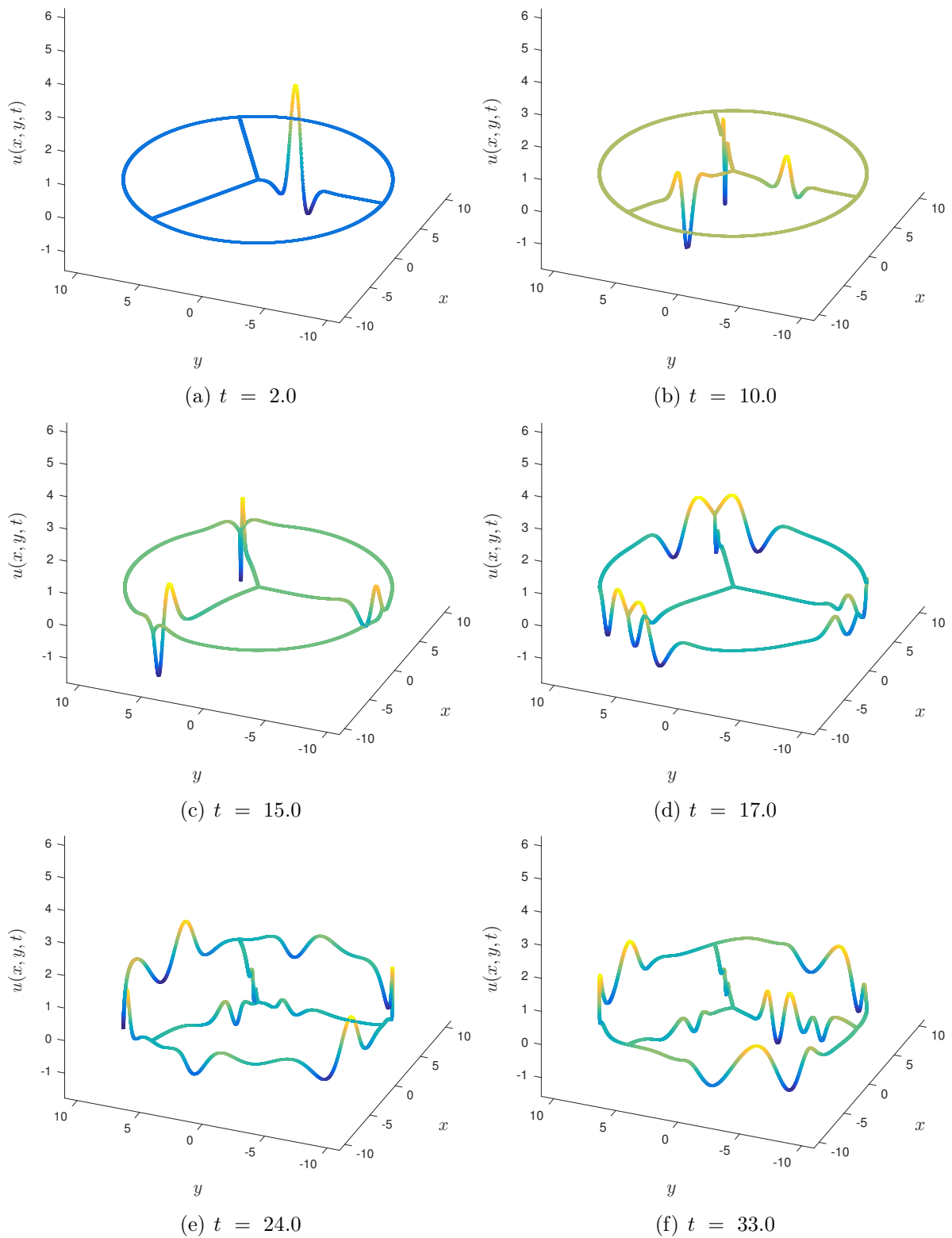


Figure 8. Evolution of a sine-Gordon breather with $c_0 = 0.95$ and $\omega = \frac{\sqrt{2}}{2}$ on the graph G_0 .

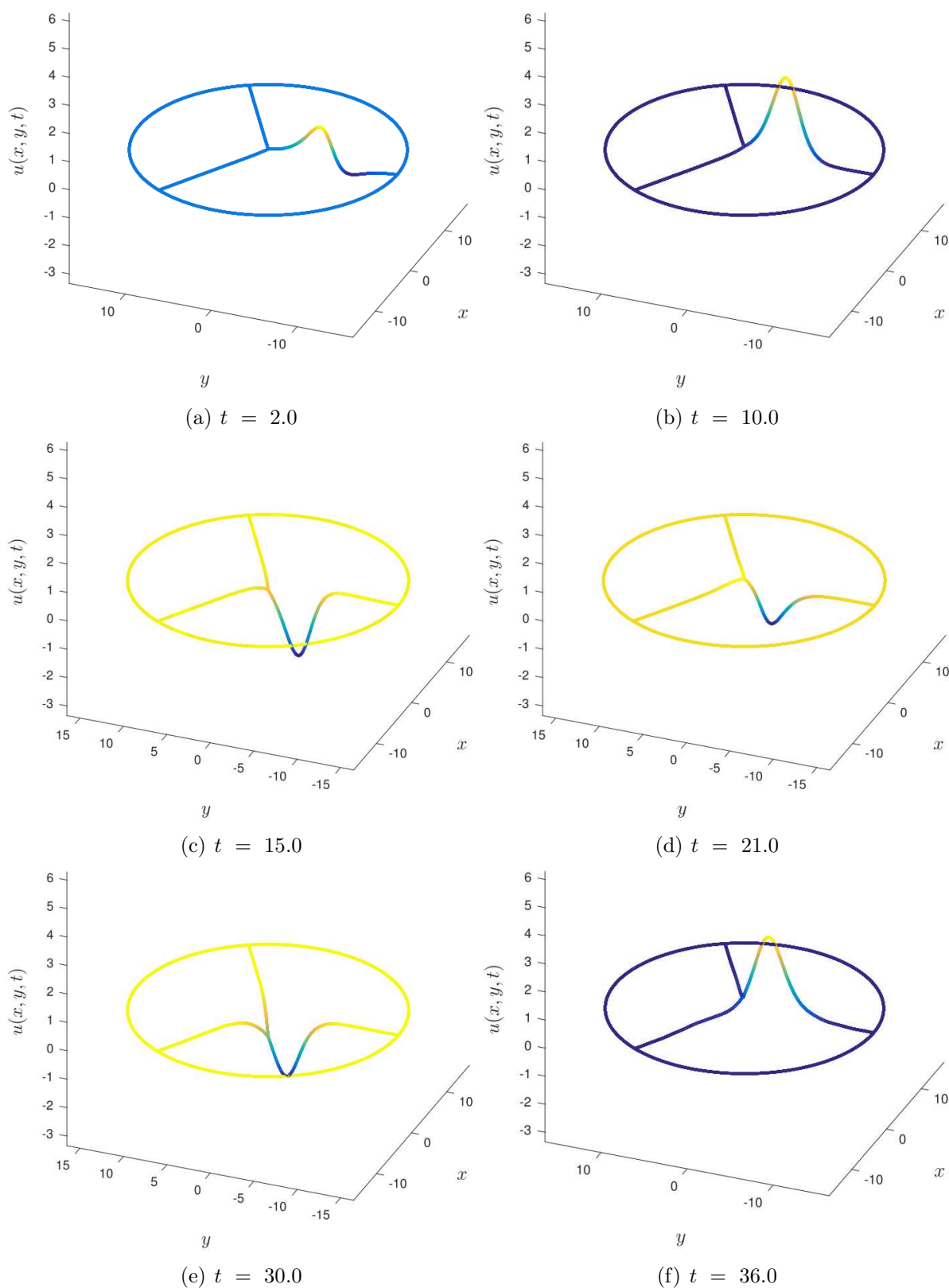


Figure 9. Evolution of a sine-Gordon 'weak' energy breather on the graph G_0 with parameters given in Table 2.

<i>Parameter</i>	<i>Value</i>
Breather speed, c_0	0.95; 0.25
Breather frequency, $\cos(\mu)$	$\frac{\sqrt{2}}{2}$, <i>i.e.</i> $\mu = \frac{\pi}{4}$
Breather energy, \mathcal{E}	11.68
Time step, Δt	0.0075
Final simulation time, T	36.0
Number of time steps, N_t	4 800
Number of points, N	1 000
Spatial discretization step, Δx	0.015

Table 2. *Parameters used in the numerical simulation of the breather propagation on a network. The breather speeds are chosen in order to illustrate the phenomena of transition/reflection through/at the junction. The number of time steps is chosen to have sufficient accuracy by verifying the stability conditions.*

The numerical results revealed a sequence of topological changes during the collisions of elementary sG kinks at the graph vertices. We considered two different situations when the kinks initially were super- and sub-critical. In the latter case the system dynamics is restricted only to a sub-graph since the kinks do not possess enough energy to go through the junctions. We also studied the dynamics of a breather in such a network. To our knowledge, these results are presented for the first time and shed light on a type of soliton turbulence.

Acknowledgments

The authors acknowledge the “Centre de Ressources Informatiques de HAUTE NORMANDIE” where most of the calculations were done. Moreover, we thank Professor Michel RAIBAUT (LAMA UMR #5127, Université SAVOIE MONT BLANC) for stimulating discussions on various geometrical matters.

A. Conservation laws approach

A weaker version of condition (2.9) can be derived from variational considerations by following [5]. Let us consider again the LAGRANGIAN density (2.2). By using the TAYLOR

expansion for the potential energy term, the LAGRANGIAN density \mathcal{L}_{sg} can be rewritten as

$$\mathcal{L}_{sG} = \underbrace{\frac{1}{2}(u_t^2 - u_x^2) - \frac{1}{2}u^2}_{\mathcal{L}_{KG}} + \sum_{k=2}^{\infty} (-1)^k \frac{u^{2k}}{(2k)!} = \mathcal{L}_{KG} + \sum_{k=2}^{\infty} (-1)^k \frac{u^{2k}}{(2k)!}.$$

The last form of the LAGRANGIAN density is particularly suitable for the complexification of the sG equation which derives from the following LAGRANGIAN

$$\mathcal{L}_{sG}^c = \frac{1}{2}(u_t u_t^* - u_x u_x^*) - \frac{1}{2}u u^* + \sum_{k=2}^{\infty} (-1)^k \frac{(u u^*)^k}{(2k)!}, \quad (\text{A.1})$$

where $u^*(x, t)$ is the complex conjugate of $u(x, t)$ (in the complex-valued version of the sG equation).

Consider now a complex-valued field $u(x, t) : \mathbb{R} \times \mathbb{R}^+ \mapsto \mathbb{C}$ whose behaviour is described by LAGRANGIAN density (A.1). The energy-momentum tensor $\mathbb{T} = (\mathcal{T}^{\alpha\beta})$ of the field $u(x, t)$ satisfies the following conservation laws

$$\partial_\alpha \mathcal{T}^{\alpha\beta} = 0, \quad (\text{A.2})$$

where $\partial_0 \stackrel{\text{def}}{=} \partial_t$, $\partial_1 \stackrel{\text{def}}{=} \partial_x$. The components of tensor \mathbb{T} are given in [33]

$$\mathcal{T}^{\alpha\beta} = \frac{\delta \mathcal{L}_{sG}^c}{\delta(\partial_\alpha u)} \partial^\beta u + \frac{\delta \mathcal{L}_{sG}^c}{\delta(\partial_\alpha u^*)} \partial^\beta u^* - g^{\alpha\beta} \mathcal{L}_{sG}^c, \quad \alpha, \beta = 0, 1, \quad (\text{A.3})$$

where $g^{\alpha\beta} \stackrel{\text{def}}{=} \text{diag}\{1, -1\}$ is the MINKOWSKI tensor. The contravariant derivative operator ∂^α is related to ∂_β by $\partial^\alpha \stackrel{\text{def}}{=} g^{\alpha\beta} \partial_\beta$. It is straightforward to compute the components of \mathbb{T} from (A.3):

$$\mathcal{T}^{00} = \frac{1}{2} \partial_0 u \partial_0 u^* + \frac{1}{2} \partial_1 u \partial_1 u^* + 1 - \cos u, \quad \mathcal{T}^{01} = -(\partial_0 u \partial_1 u^* + \partial_0 u^* \partial_1 u). \quad (\text{A.4})$$

One can easily identify \mathcal{T}^{00} with the energy density and \mathcal{T}^{01} with the energy flux (see also equation (A.2)). Postulating the energy conservation on the Y -junction one obtains the following condition (see [5] for more details):

$$\mathcal{T}^{10}|_{x \rightarrow C, x \in S_1} + \mathcal{T}^{10}|_{x \rightarrow C, x \in S_2} + \mathcal{T}^{10}|_{x \rightarrow C, x \in S_3} = 0,$$

which can be expanded according to (A.4) to give finally the following analogue of the KIRCHHOFF condition:

$$\partial_t u^* \cdot (\partial^1 u + \partial^2 u + \partial^3 u) + \partial_t u \cdot (\partial^1 u^* + \partial^2 u^* + \partial^3 u^*) = 0 \text{ at } \mathbf{x} = C. \quad (\text{A.5})$$

The last condition is weaker than (2.9) in the sense that all solutions to (2.9) satisfy (A.5). However, the inverse generally is not true.

References

- [1] M. J. Ablowitz, D. J. Kaup, A. C. Newell, and H. Segur. Method for Solving the Sine-Gordon Equation. *Phys. Rev. Lett.*, 30(25):1262–1264, jun 1973. [7](#), [8](#)
- [2] R. Abraham, J. E. Marsden, and T. Ratiu. *Manifolds, Tensor Analysis, and Applications*, volume 75. Springer-Verlag, New York, 1988. [5](#)
- [3] J. Argyris, M. Haase, and J. C. Heinrich. Finite element approximation to two-dimensional sine-Gordon solitons. *Comput. Methods Appl. Mech. Engrg.*, 86(1):1–26, mar 1991. [13](#)
- [4] V. I. Arnold. *Mathematical Methods of Classical Mechanics*. Springer, New York, 2nd edition, 1997. [5](#)
- [5] P. N. Bibikov and L. V. Prokhorov. Mechanics not on a manifold. *J. Phys. A: Math. Gen.*, 42(4):045302, jan 2009. [5](#), [6](#), [9](#), [27](#), [28](#)
- [6] J. L. Bona and R. Cascaval. Nonlinear dispersive waves on trees. *Canadian Applied Mathematics Quarterly*, 16(1):1–18, 2008. [5](#)
- [7] A. Bressan, S. Canić, M. Garavello, M. Herty, and B. Piccoli. Flows on networks: recent results and perspectives. *EMS Surveys in Mathematical Sciences*, 1(1):47–111, 2014. [5](#)
- [8] J.-G. Caputo and D. Dutykh. Nonlinear waves in networks: model reduction for sine-Gordon. *Phys. Rev. E*, 90:022912, 2014. [6](#), [9](#), [13](#), [17](#), [21](#)
- [9] J.-G. Caputo, D. Dutykh, and B. Gleyse. Coupling conditions for the nonlinear shallow water equations in forks. *Submitted*, pages 1–24, 2017. [13](#)
- [10] R. Courant, K. Friedrichs, and H. Lewy. Über die partiellen Differenzgleichungen der mathematischen Physik. *Mathematische Annalen*, 100(1):32–74, 1928. [15](#)
- [11] R. F. Dashen, B. Hasslacher, and A. Neveu. Nonperturbative methods and extended-hadron models in field theory. I. Semiclassical functional methods. *Phys. Rev. D*, 10(12):4114–4129, 1974. [5](#), [23](#)
- [12] M. Dehghan and A. Shokri. A numerical method for solution of the two-dimensional sine-Gordon equation using the radial basis functions. *Math. Comp. Simul.*, 79(3):700–715, dec 2008. [13](#)
- [13] D. Dutykh and E. Pelinovsky. Numerical simulation of a solitonic gas in KdV and KdV-BBM equations. *Phys. Lett. A*, 378(42):3102–3110, aug 2014. [23](#)
- [14] L. D. Faddeev and L. Takhtajan. *Hamiltonian Methods in the Theory of Solitons*. Springer, Berlin Heidelberg New York, 1987. [6](#)
- [15] D. Furihata. Finite-difference schemes for nonlinear wave equation that inherit energy conservation property. *J. Comp. Appl. Math.*, 134(1-2):37–57, sep 2001. [13](#)
- [16] R. Gould. *Graph Theory*. Dover Publications Inc., dover edition, 2012. [5](#), [15](#)
- [17] A. Grunnet-Jepsen, F. N. Fahrenndorf, S. A. Hattel, N. Grønbech-Jensen, and M. R. Samuelsen. Fluxons in three long coupled Josephson junctions. *Phys. Lett. A*, 175(2):116–120, apr 1993. [5](#)

- [18] D. Gulevich and F. Kusmartsev. Flux Cloning in Josephson Transmission Lines. *Phys. Rev. Lett.*, 97(1):017004, jul 2006. [9](#), [21](#)
- [19] D. Gulevich, F. Kusmartsev, S. Savel'ev, V. Yampol'skii, and F. Nori. Shape Waves in 2D Josephson Junctions: Exact Solutions and Time Dilation. *Phys. Rev. Lett.*, 101(12):127002, sep 2008. [21](#)
- [20] A. Haefliger. Feuilletages sur les variétés ouvertes. *Topology*, 9(2):183–194, may 1970. [9](#)
- [21] S. A. Hattel, A. Grunnet-Jepsen, and M. R. Samuelsen. Dynamics of three coupled long Josephson junctions. *Phys. Lett. A*, 221(1-2):115–123, sep 1996. [5](#), [21](#)
- [22] M. Ilati and M. Dehghan. The use of radial basis functions (RBFs) collocation and RBF-QR methods for solving the coupled nonlinear sine-Gordon equations. *Engineering Analysis with Boundary Elements*, 52:99–109, mar 2015. [13](#)
- [23] A. L. Islas and C. M. Schober. Multi-symplectic Spectral Methods for the Sine-Gordon Equation. In P. M. A. Sloom, D. Abramson, A. V. Bogdanov, Y. E. Gorbachev, J. J. Dongarra, and A. Y. Zomaya, editors, *Computational Science - ICCS 2003*, pages 101–110. Springer, Berlin, Heidelberg, 2003. [7](#)
- [24] G. Khakinzyanov and D. Dutykh. On supraconvergence phenomenon for second order centered finite differences on non-uniform grids. *J. Comp. Appl. Math.*, 326:1–14, dec 2017. [17](#)
- [25] B. Leimkuhler and S. Reich. *Simulating Hamiltonian Dynamics*, volume 14 of *Cambridge Monographs on Applied and Computational Mathematics*. Cambridge University Press, Cambridge, 2005. [13](#), [14](#)
- [26] A. Lew, J. Marsden, M. Ortiz, and M. West. An overview of variational integrators. In *Finite Element Methods: 1970s and beyond (CIMNE, 2003)*, page 18, Barcelona, Spain, 2004. [13](#)
- [27] J. E. Marsden, G. W. Patrick, and S. Shkoller. Multisymplectic geometry, variational integrators, and nonlinear PDEs. *Comm. Math. Phys.*, 199(2):351–395, 1998. [13](#)
- [28] F. A. Mehmeti and V. Régnier. Splitting of energy of dispersive waves in a star-shaped network. *ZAMM*, 83(2):105–118, feb 2003. [9](#)
- [29] B. Moore and S. Reich. Backward error analysis for multi-symplectic integration methods. *Numerische Mathematik*, 95(4):625–652, 2003. [15](#)
- [30] K. Nakajima and Y. Onodera. Logic design of Josephson network. II. *J. Appl. Phys.*, 49(5):2958, 1978. [5](#)
- [31] K. Nakajima, Y. Onodera, and Y. Ogawa. Logic design of Josephson network. *J. Appl. Phys.*, 47(4):1620–1627, apr 1976. [5](#)
- [32] J. Rashidinia and R. Mohammadi. Tension spline solution of nonlinear sine-Gordon equation. *Numerical Algorithms*, 56(1):129–142, jan 2011. [13](#)
- [33] L. H. Ryder. *Quantum Field Theory*. Cambridge University Press, Cambridge, 2nd edition, 1996. [28](#)
- [34] A. Scott. *Nonlinear Science: Emergence and Dynamics of Coherent Structures*. Oxford University Press, 2nd edition, 2003. [6](#)
- [35] A. Scott. *Encyclopedia of Nonlinear Science*. Routledge, New-York, 2004. [6](#), [8](#)

- [36] H. Susanto and S. A. van Gils. Existence and stability analysis of solitary waves in a tricrystal junction. *Phys. Lett. A*, 338(3-5):239–246, may 2005. 5
- [37] L. A. Takhtadzhyan and L. D. Faddeev. Essentially nonlinear one-dimensional model of classical field theory. *Theor. Math. Phys.*, 21(2):1046–1057, 1974. 5, 23
- [38] Y. Vassilevskii, S. Simakov, V. Salamatova, Y. Ivanov, and T. Dobroserdova. Numerical issues of modelling blood flow in networks of vessels with pathologies. *Russ. J. Numer. Anal. Math. Modelling*, 26(6):605–622, 2011. 5
- [39] J. A. D. Wattis. Variational approximations to breathers in the discrete sine-Gordon equation II: moving breathers and Peierls-Nabarro energies. *Nonlinearity*, 9(6):1583–1598, nov 1996. 8
- [40] V. E. Zakharov, A. N. Pushkarev, V. F. Shvets, and V. V. Yankov. Soliton turbulence. *JETP Lett.*, 48(2):79–82, 1988. 23
- [41] E. Zuazua. Control and stabilization of waves on 1-d networks. *Lecture Notes in Mathematics*, 2062:463–493, 2013. 5

D. DUTYKH: LAMA, UMR 5127 CNRS, UNIVERSITÉ SAVOIE MONT BLANC, CAMPUS SCIENTIFIQUE, F-73376 LE BOURGET-DU-LAC CEDEX, FRANCE AND UNIV. GRENOBLE ALPES, UNIV. SAVOIE MONT BLANC, CNRS, LAMA, 73000 CHAMBÉRY, FRANCE

E-mail address: Denys.Dutykh@univ-savoie.fr

URL: <http://www.denys-dutykh.com/>

J.-G. CAPUTO: LABORATOIRE DE MATHÉMATIQUES, INSA DE ROUEN, BP 8, AVENUE DE L'UNIVERSITÉ, SAINT-ETIENNE DU ROUVRAY, F-76801 FRANCE

E-mail address: caputo@insa-rouen.fr

URL: <https://sites.google.com/site/jeanguycaputo/>